


RESEARCH

Open Access



Investigating Various Factors Affecting the Long-Term Compressive Strength of Heat-Cured Fly Ash Geopolymer Concrete and the Use of Orthogonal Experimental Design Method

Hongen Zhang^{1,2}, Lang Li¹, Prabir Kumar Sarker², Tao Long¹, Xiaoshuang Shi^{1*}, Qingyuan Wang^{1,3*}  and Gaochuang Cai⁴

Abstract

This work quantified the hierarchy of the influence of three common mixture design parameters on the compressive strength and the rate of strength increase over the long term of low-calcium fly ash geopolymer concrete (FAGC) through designing 16 mixtures by the orthogonal experimental design (OED) method. The parameters used in the study were liquid to fly ash (L/FA) ratio, sodium hydroxide concentration (SHC) and sodium silicate solution to sodium hydroxide solution (SS/SH) ratio. The L/FA ratio showed little effect on compressive strength when it was varied from 0.40 to 0.52. SHC showed the greatest influence on compressive strength with little impact on the rate of strength increase after the initial heat curing. Even though the SS/SH ratio showed a small effect on the initial compressive strength, it had a considerable influence on the rate of strength increase over the long term. It was found that the compressive strength at 480 days was positively related to the $\text{Na}_2\text{O}/\text{SiO}_2$ molar ratio when it was varied from 0.49 to 0.80 and the Si/Al molar ratio was increased up to 1.87. Analysis of the failure types of specimens demonstrated that compressive strength of FAGC was associated with the strength of the mortar–aggregate interface zone (MAIZ).

Keywords: orthogonal experimental design (OED), geopolymer concrete, mortar–aggregate interface zone (MAIZ), $\text{Na}_2\text{O}/\text{SiO}_2$ molar ratios, Si/Al molar ratio

1 Introduction

Nowadays, geopolymer binder is attracting a growing interest as an alternative to cement for concrete production. It has been shown that geopolymer concrete exhibits its compressive strength which is comparable with that of cement-based (Jo et al. 2016; Pasupathy et al. 2018; Nazari et al. 2019).

Fly ash has been widely used as the raw material to produce geopolymer due to its abundant silicon and aluminum elements, suitable shape and size distribution (Riahi and Nazari 2012; Kotwal et al. 2015). Fly ash-based geopolymer concrete (FAGC) is made of low-calcium fly ash geopolymer binder and normal concrete aggregates. The properties of FAGC is affected by different factors such as CaO content, curing conditions, sodium hydroxide (NaOH) concentration, ratio of alkali-activator liquid to fly ash and the ratio of sodium silicate (Na_2SiO_3) to NaOH solutions. Previous researches (Shi et al. 2012; de Vargas et al. 2011; Sindhunata et al. 2006; Hongen et al. 2017; Zhang et al. 2018) found out higher curing temperatures (up to 80 °C) has a positive effect on compressive

*Correspondence: shixs@scu.edu.cn; wangqy@scu.edu.cn

¹ Key Laboratory of Deep Underground Science and Engineering (Ministry of Education), School of Architecture and Environment, Sichuan University, Chengdu 610065, China

Full list of author information is available at the end of the article
Journal information: ISSN 1976-0485 / eISSN 2234-1315

strength of FAGCs. Studies (Chithambaram et al. 2018; Nath and Sarker 2015) attributed appropriate NaOH concentration and the ratio of Na₂SiO₃ to NaOH solution to high compressive strength of geopolymer concrete. However, it is necessary to clearly quantify the influence of these parameters on the properties of FAGC. The influence of different types of fly ash on the long-term strength of FAGC were studied by Gunasekara et al. (2017). It is also important to assess the influence of the other geopolymer mix design parameters on the long-term properties of FAGCs. The orthogonal experimental design (OED) method has been widely used in different areas (Ji et al. 2014; Zhu et al. 2013; Yang et al. 2011) since it is considered as an efficient method to provide maximum and reliable information by designing fewer possible groups.

Based on the above discussions, the main aim of this research is to resort to the statistical *P*-value to quantify the hierarchy of the influence of three important factors namely liquid to fly ash ratio, sodium hydroxide concentration and sodium silicate solution to sodium hydroxide solution ratio on the compressive strength and the rate of compressive strength increase over the long term. The use of orthogonal experimental design method is also evaluated using the test results.

2 Experimental Procedure

2.1 Materials

2.1.1 Aggregates

The particle size of locally available coarse aggregate is in the range of 4.75 mm and 22 mm and that of river sand is smaller than 4 mm. The physical properties of coarse and fine aggregates are presented in Table 1.

2.1.2 Fly Ash

A low-calcium fly ash was used as the raw material to provide the essential silicon and aluminum for synthesis of geopolymer binder. It can be seen from Fig. 1 that the fly ash particles were in a spherical shape. The results of JL-6000 laser particle size analyzer showed that the average particle size of fly ash was 13.5 micron. The particle size distribution of fly ash is presented in Fig. 2. The chemical compositions and loss on ignition (LOI) of fly ash are given in Table 2.

Table 1 The physical properties of coarse aggregate and sand.

Aggregate	Packing density (kg/m ³)	Apparent density (kg/m ³)	Water content (%)
Coarse aggregate	1479	2632	0.3
Fine aggregate	1342	2381	0.1

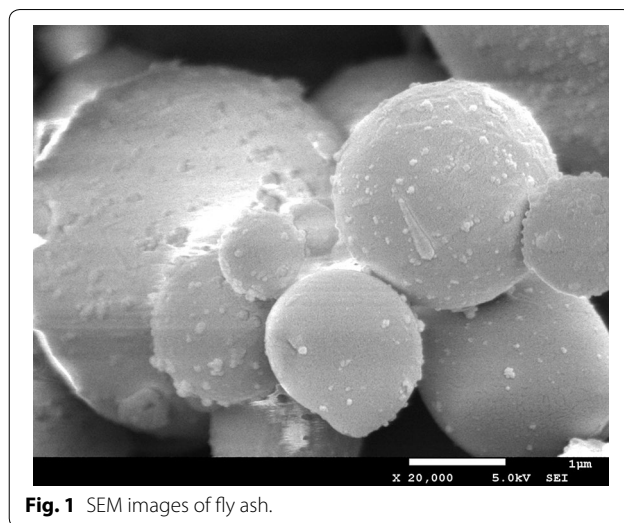


Fig. 1 SEM images of fly ash.

2.1.3 Alkali-Activator Solution

The alkali-activator solution consisted of sodium silicate (Na₂SiO₃) and sodium hydroxide (NaOH) solutions. The Na₂SiO₃ solution has a modulus ratio (*M_s*) equaling to 3.23 (where *M_s* = SiO₂/Na₂O, Na₂O = 8.83%, SiO₂ = 27.64%). The NaOH solution was made by dissolving NaOH particles of 98% purity into distilled water. The alkali-activator solution was placed at room temperature for about 24 h before use.

2.2 Specimen Preparation

2.2.1 Mixture Design

This paper investigated the effects of three mix design parameters which are (A): liquid/fly ash (L/FA) ratio, (B): sodium hydroxide concentration (SHC) and (C): sodium silicate solution to sodium hydroxide solution (SS/

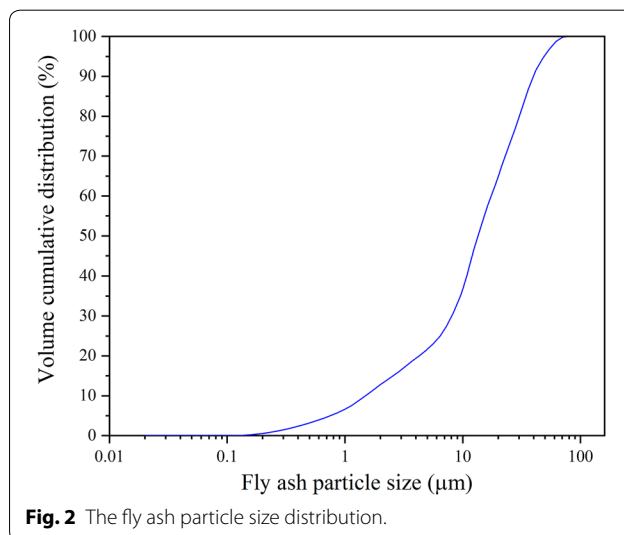


Fig. 2 The fly ash particle size distribution.

Table 2 Chemical compositions of fly ash.

Chemical composition	SiO ₂	Al ₂ O ₃	CaO	Fe ₂ O ₃	MgO	K ₂ O	SO ₃	TiO ₂	Na ₂ O	LOI ^a
Fly ash (%)	50.76	27.32	5.4	4.64	3.72	4.85	2.0	1.16	0.8	2.83

^a Loss on ignition.

Table 3 The mix design variables.

Level	Variables		
	A (L/FA)	B (SHC) (mol)	C (SS/SH)
1	0.40	8	2.0
2	0.44	10	2.5
3	0.48	12	3.1
4	0.52	14	4.0

Table 4 The orthogonal experimental design variables.

Mix no.	Mix designation	A (L/FA)	B (SHC) (mol)	C (SS/SH)
1	A1B1C1	0.40	8	2.0
2	A1B2C2	0.40	10	2.5
3	A1B3C3	0.40	12	3.1
4	A1B4C4	0.40	14	4.0
5	A2B1C2	0.44	8	2.5
6	A2B2C1	0.44	10	2.0
7	A2B3C4	0.44	12	4.0
8	A2B4C3	0.44	14	3.1
9	A3B1C3	0.48	8	3.1
10	A3B2C4	0.48	10	4.0
11	A3B3C1	0.48	12	2.0
12	A3B4C2	0.48	14	2.5
13	A4B1C4	0.52	8	4.0
14	A4B2C3	0.52	10	3.1
15	A4B3C2	0.52	12	2.5
16	A4B4C1	0.52	14	2.0

SH) ratio. Each factor has four different levels as given in Table 3. The values of factor A increased from 0.40 to 0.52 with 0.04 incremental steps and the molarity of sodium hydroxide (NaOH) varied from 8 to 14 M with 2 M incremental steps. The values of SS/SH ratio were 2.0, 2.5, 3.1 and 4.0.

According to the OED principle of L₁₆ (4³), a total of 16 mixtures were prepared (Table 4). The concrete mixture proportions together with Si/Al molar ratios and Na₂O/SiO₂ molar ratios are given in Table 5. The Si/Al molar ratios were calculated from the silicon and aluminum available in fly ash and sodium silicate solution. The Na₂O/SiO₂ molar ratios were calculated from the silicon dioxide and sodium oxide from the alkali-activator solution.

2.2.2 Casting and Curing of Test Specimens

The mixing of geopolymer concrete was conducted in a concrete mixer at room temperature. The aggregates and fly ash were first dry-mixed in the mixer for about 3 min. The alkali-activator solution was gradually added and the wet-mixing continued for another 5 min. The fresh geopolymer concrete was poured into steel cubic moulds in two equal layers. The concrete samples were vibrated on a vibrating table.

After finishing, the moulds were covered with plastic film and then cured in an oven at a temperature of 80 °C. After heat curing for 24 h, the specimens were removed from the oven and demoulded. According to the GB/T50081-2002 (Ministry of Construction of the PRC & General Administration of Quality Supervision, Inspection and Quarantine of the People's Republic of China 2003), the specimens were stored at 20 °C and 97% relative humidity until the testing.

2.3 Test Procedure

2.3.1 Compressive Strength Test

Compressive strength tests were carried out at a load rate of 0.5 MPa/s using 2000 kN electro-hydraulic mechanical testing machine referring to the GB/T50081-2002 (Ministry of Construction of the PRC & General Administration of Quality Supervision, Inspection and Quarantine of the People's Republic of China 2003). The test was conducted using cubic specimens of 100 mm in dimensions.

2.3.2 Scanning Electron Microscopy (SEM) and Energy Dispersive Spectroscopy (EDS) Test

The concrete samples of M13 to M16 were selected to carry out scanning electron microscopy (SEM) and energy dispersive spectroscopy (EDS) using SU3500 instrument in Sichuan University, China. The sample's surface was coated with a layer of platinum using a sputter coater with 15 mA currents for duration of 90 s before the SEM and EDS analysis.

2.3.3 Thermogravimetric Analysis (TGA) and Derivative Thermogravimetric Analysis (DTG)

At the curing age of 480 days, fragments of M13 to M16 concrete specimens were ground into powder and then heated to about 800 °C at a constant heating rate of 10 °C/min in the same gas environment. Thermogravimetric

Table 5 Mix proportions of FAGC (kg/m³).

Mix no.	CA ^a	S ^b	FA ^c	SS ^d	SH ^e	Na ₂ O/SiO ₂	Si/Al
1	1212	544	460	122.7	61.3	0.66	1.81
2	1212	544	460	131.4	52.6	0.65	1.82
3	1212	544	460	139.1	44.9	0.63	1.84
4	1212	544	460	147.2	36.8	0.58	1.85
5	1201	539	460	142.9	57.2	0.59	1.85
6	1201	539	460	133.4	66.7	0.74	1.83
7	1201	539	460	160.1	40.0	0.55	1.88
8	1201	539	460	151.3	48.8	0.66	1.86
9	1186	533	460	166.9	53.9	0.54	1.89
10	1186	533	460	176.6	44.2	0.52	1.91
11	1186	533	460	147.2	73.6	0.80	1.85
12	1186	533	460	157.7	63.1	0.75	1.87
13	1174	527	460	191.4	47.8	0.49	1.94
14	1174	527	460	180.9	58.3	0.58	1.92
15	1174	527	460	170.9	68.3	0.70	1.90
16	1174	527	460	159.5	79.7	0.86	1.88

^a Coarse aggregate.^b Sand.^c Fly ash.^d Na₂SiO₃ solution.^e NaOH solution.

analysis (TGA) and derivative thermogravimetric analysis (DTG) were conducted using a METTLER TOLEDO TGA/DSC2/1600 instrument in a nitrogen environment (N₂ flowing at 50 ml/min).

3 Test Results and Discussions

3.1 Compressive Strength

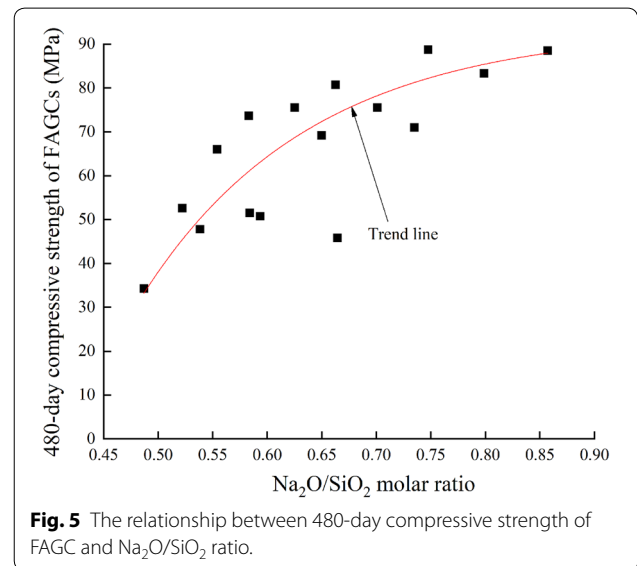
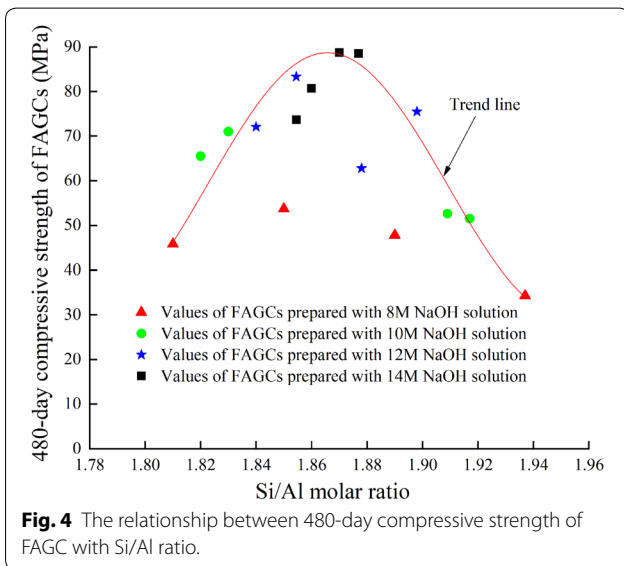
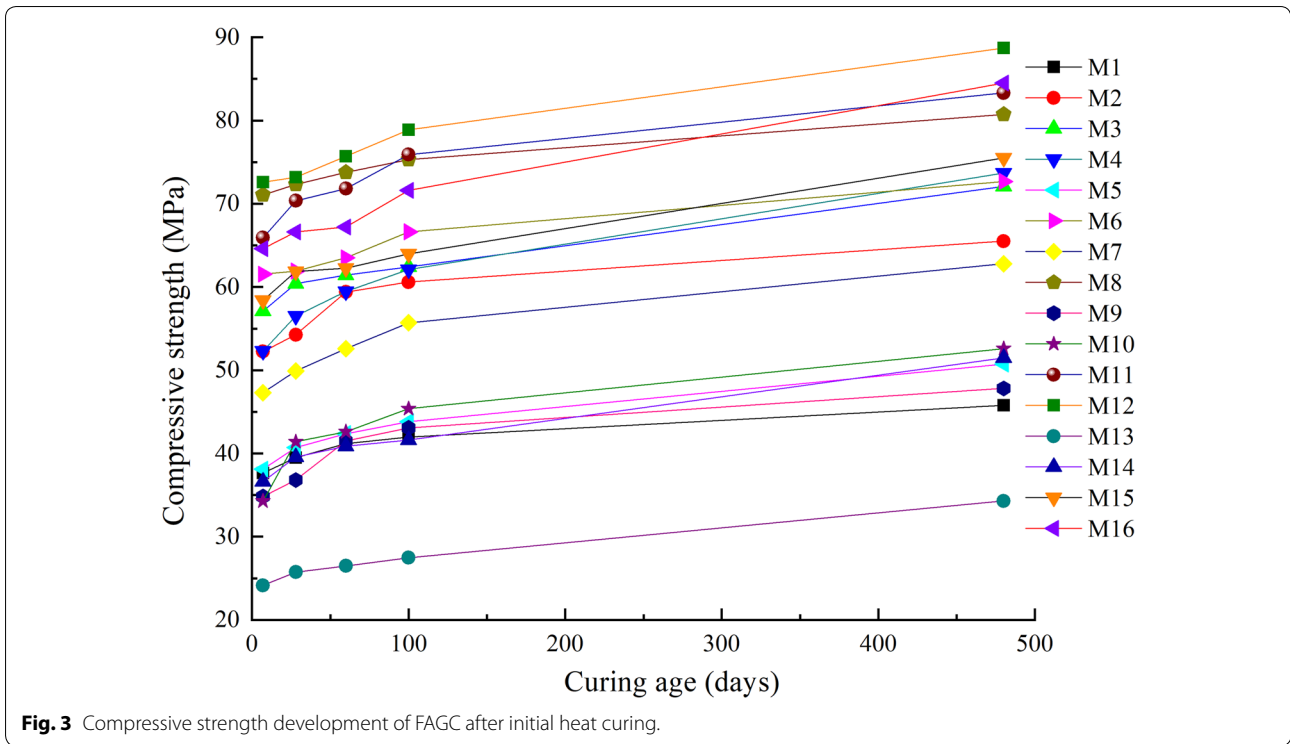
The compressive strength of mixtures 1 to 16 at the ages of 7, 28 and 480 days were presented in Table 6. Additionally, the strength development at the ages of 7, 28, 60, 100 and 480 days were also plotted in Fig. 3. It can be seen from Fig. 3 that compressive strength of all the mixtures increased with the increase of age after the initial 24 h heat curing at 80 °C and mixture 12 reached the highest compressive strength. In the light of this compressive strength value, the best concrete mixture was A₃B₄C₂, which meant that L/FA ratio was at level 3, SHC was at level 4 and SS/SH ratio was at level 2.

The compressive strengths up to 480 days, presented in Table 6, were used to investigate the long term compressive strength development of low-calcium FAGC. Figure 4 shows that 480-day compressive strength of FAGC plotted against the Si/Al molar ratio. The FAGC mixtures had a narrow range of Si/Al molar ratios (ranging from 1.81 to 1.94) and the influence of Si/Al ratio on compressive strength could be observed. Compressive strength was first observed to increase with the increase in Si/Al

Table 6 Compressive strength of FAGCs.

Compressive strength of FAGCs (MPa)			
Mix no.	7-day	28-day	480-day
1	37.6 ± 0.9	39.5 ± 4.6	45.8 ± 0.7
2	52.2 ± 2.7	54.3 ± 1.5	65.5 ± 4.0
3	57.1 ± 5.4	60.4 ± 1.8	72.1 ± 5.3
4	52.3 ± 6.6	56.5 ± 3.4	73.7 ± 2.3
5	38.1 ± 1.6	40.7 ± 2.9	50.7 ± 3.2
6	61.5 ± 4.6	61.9 ± 5.9	71.0 ± 6.6
7	47.3 ± 3.3	49.9 ± 1.5	62.8 ± 4.7
8	71.1 ± 0.8	72.3 ± 2.1	80.7 ± 2.5
9	34.8 ± 1.0	36.8 ± 1.2	47.8 ± 0.9
10	34.3 ± 0.8	41.4 ± 2.9	52.6 ± 3.1
11	65.9 ± 1.8	70.4 ± 7.7	83.3 ± 0.4
12	72.6 ± 0.5	73.2 ± 4.3	88.7 ± 3.2
13	24.1 ± 0.6	25.7 ± 0.6	34.3 ± 0.4
14	36.6 ± 1.2	39.6 ± 0.7	51.5 ± 2.7
15	58.4 ± 1.5	61.9 ± 1.1	75.5 ± 1.1
16	64.6 ± 3.3	66.6 ± 6.3	84.5 ± 2.5

ratio and FAGC with Si/Al ratio close to 1.87 tended to show high compressive strength. A distinct decrease was observed in compressive strength when the Si/Al ratio was larger than 1.87. The compressive strength of FAGCs



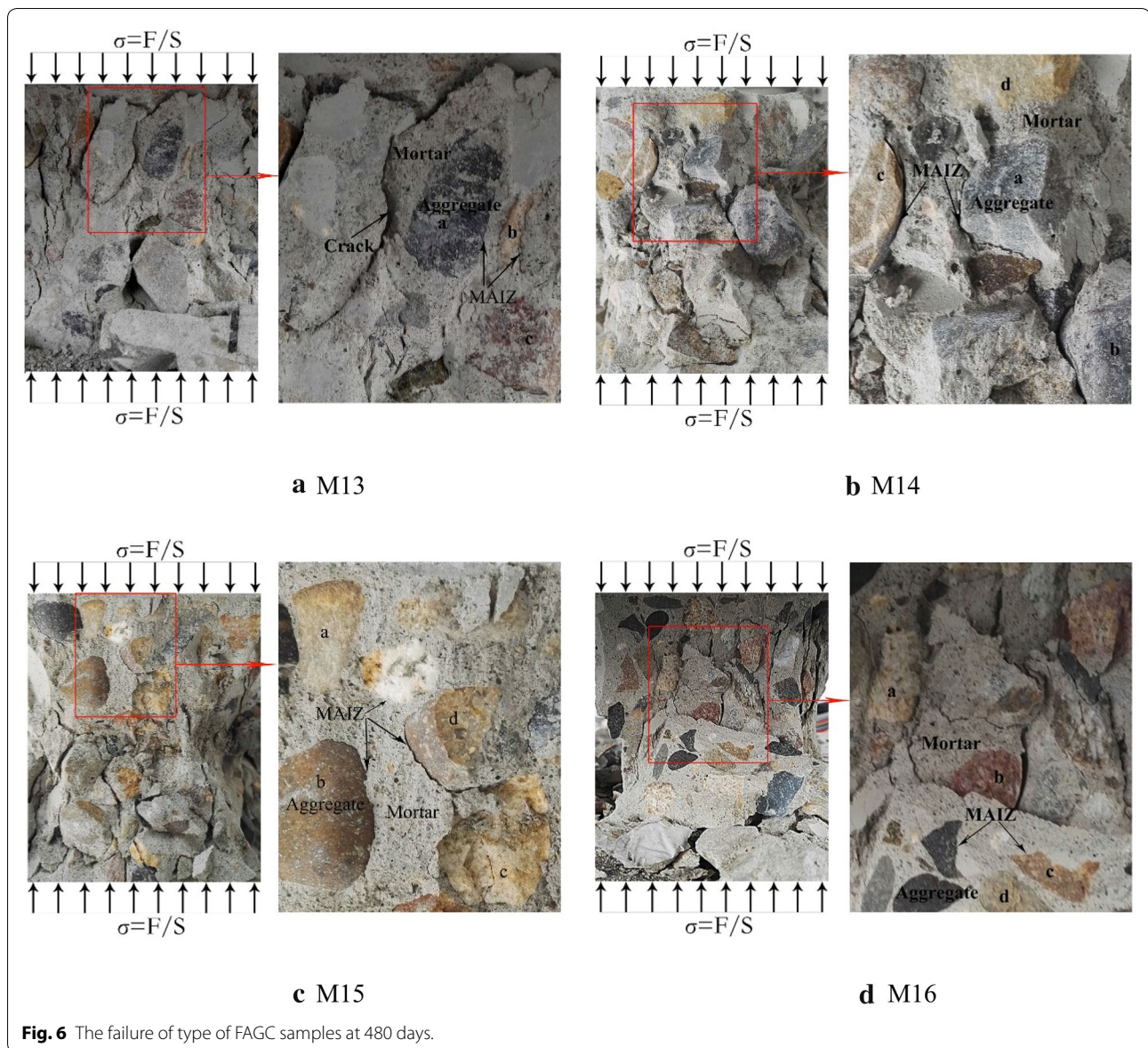
prepared with NaOH solutions of different molarity are also noted in Fig. 4. To some degree, the influence of Si/Al molar ratio on the long-term compressive strength was affected by the concentration of NaOH solution.

The compressive strengths of FAGCs at 480 days as a function of $\text{Na}_2\text{O}/\text{SiO}_2$ molar ratios are presented in Fig. 5. It can be seen from Fig. 5 that compressive strength increased with the increase in $\text{Na}_2\text{O}/\text{SiO}_2$ molar

ratio. This is attributed to the hypothesis that increasing the Na_2O increases the binding mechanism and properties development of geopolymers (Chi and Huang 2013).

3.2 The Failure Pattern of Concrete

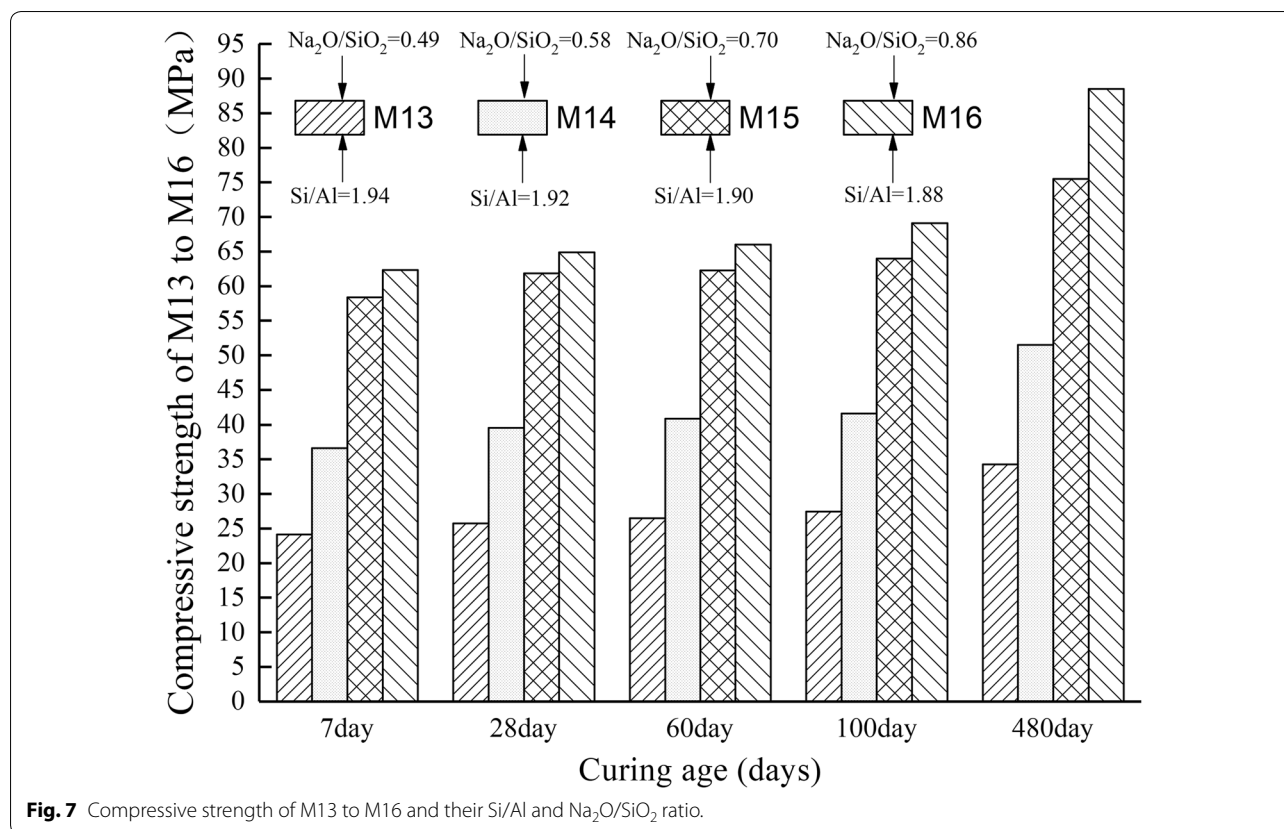
Figure 6 showed the failure patterns of the mortar, aggregates and mortar–aggregate interface zone (MAIZ) of the specimens of mixtures 13, 14, 15 and 16, respectively. The



coarse aggregate and MAIZ remained intact in mixture 13 (referring to the letter a, b and c in Fig. 6a). Therefore, the compressive strength of the concrete of mixture 13 depended on the strength of mortar. As can be seen in Fig. 6b, the MAIZ were broken and several aggregates were observed to have been pulled out under pressure (referring to the letters c and d in Fig. 6b), which demonstrated that the compressive strength of mixture 14 is determined by the strength of MAIZ. It was observed from Fig. 6c that almost all the coarse aggregates were pulled out and the MAIZ were almost still in their integrity. The MAIZ were in perfect conditions and all the coarse aggregates were pulled out in mixture 16 (Fig. 6d). However, several cracks were still observed in Fig. 6d,

which was believed to be caused by explosive spalling under the increasing external load. The failure-status of specimens in Fig. 6c, d demonstrated that the compressive strength of concrete depended to a great extent on the strength of coarse aggregate. The distinct difference in the failure-status of the mortar, aggregates and MAIZ indicated that the higher SHC and lower SS/SH ratio could improve the strength of mortar and MAIZ.

The compressive strengths of mixtures 13, 14, 15 and 16 at different ages are also presented in Fig. 7. The results show that the compressive strength of FAGC increased with the curing time. It could be observed from Fig. 7 that the compressive strength of mixture 16 was the largest at all the curing ages, followed by the compressive strengths



of mixtures 15, 14 and 13. It is concluded from Figs. 6 and 7 that the compressive strength of concrete was associated with the failure type of concrete. In fact, the change in SHC and SS/SH ratio led to the variation in Na₂O/SiO₂ and Si/Al molar ratios. The Na₂O/SiO₂ and Si/Al molar ratio values corresponding to the four mixtures are also presented in Fig. 7. This figure shows that the compressive strength increased with the increase in Na₂O/SiO₂ molar ratio and the decrease in Si/Al molar ratio. Together with the failure patterns (Fig. 6), it was found that increasing the Na₂O content and decreasing the Si/Al ratio could enhance the binding strength of MAIZ. Furthermore, the low Na₂O/SiO₂ molar ratio value meant the high content of the sodium silicate solution, causing the geopolymer concrete to become sticky due to the viscous characteristics of the sodium silicate solution. The high amounts of the sodium silicate solution might hinder the geopolymerization process (Heah et al. 2012).

3.3 Microstructures

The samples of M13, M14, M15 and M16 at 480 days were investigated by using SEM and EDS. The SEM and EDS results of M13 to M16 at 480 days were used to find out how the NaOH molarity affects the long-term compressive strength of geopolymer concrete in the micro-level. The

results of SEM are presented in Fig. 8. It is observed from Fig. 8 that the formation of geopolymer gels presented different shapes. The gel in Fig. 8a looked like slices in the concrete. The shape of the gel in Fig. 8b was like coarse strip with several small voids. A kind of shale-like gel was observed in Fig. 8c, d. The difference between the shapes of Fig. 8c, d was that much more void spaces could be observed in Fig. 8c and the gel in Fig. 8d was denser than that in Fig. 8c. Together with the 480-day compressive strength of M13 to M16 presented in Fig. 7, it could be noted that the compressive strength was associated with the morphology of microstructure. The morphological change is mainly attributed to the increase of concentration of NaOH solution. The amounts of leaching Si and Al from raw materials increased with the increase of NaOH molarity, which was also reported by other researchers (Xu et al. 2001). Therefore, FAGCs prepared with higher molarity of NaOH solution experienced a more complete geopolymerization. As a result, more geopolymer product could be observed in Fig. 8c, d, which is evidenced by the EDS results presented in Fig. 9.

The gels shown in Fig. 8 were also investigated by EDS and the results are presented in Fig. 9 and Table 7. The results of EDS showed that the elements of the gel were O, Na, Al, Si and K. The Si/Al weight ratio and Si/

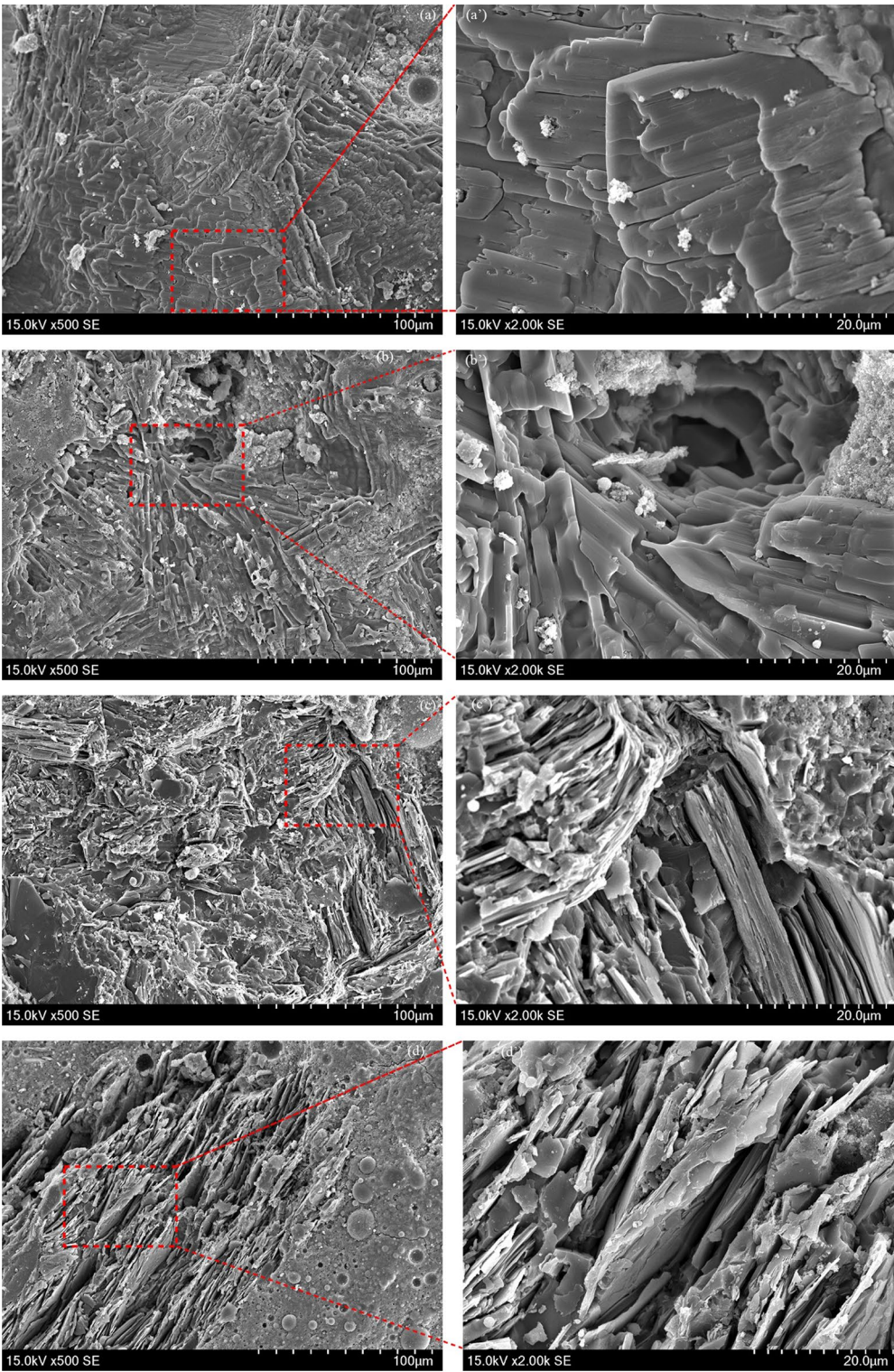


Fig. 8 SEM images of FAGC samples at 480 days (a–d corresponding to M13–M16).

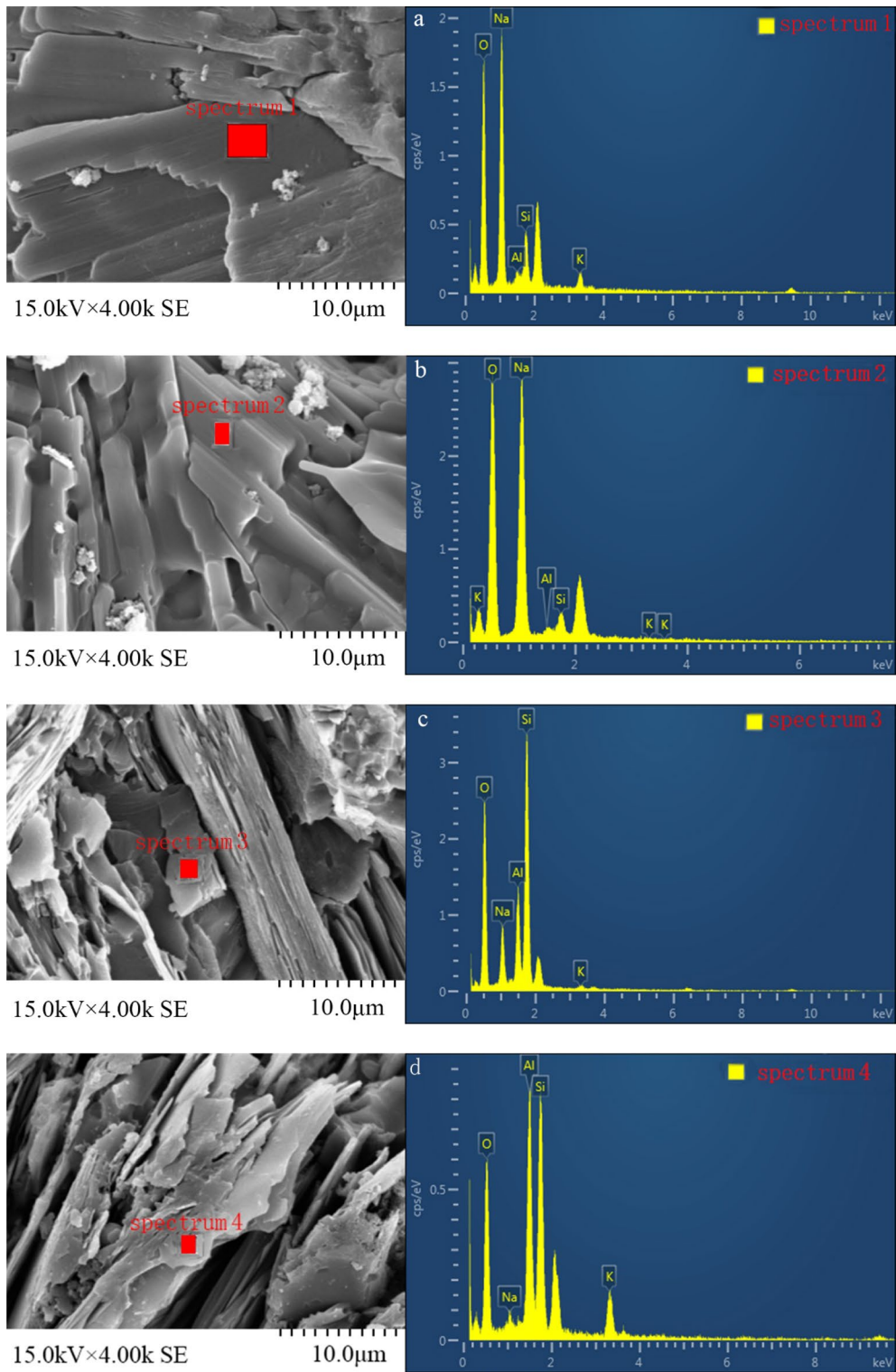


Fig. 9 The EDS results of **a** M13, **b** M14, **c** M15 and **d** M16.

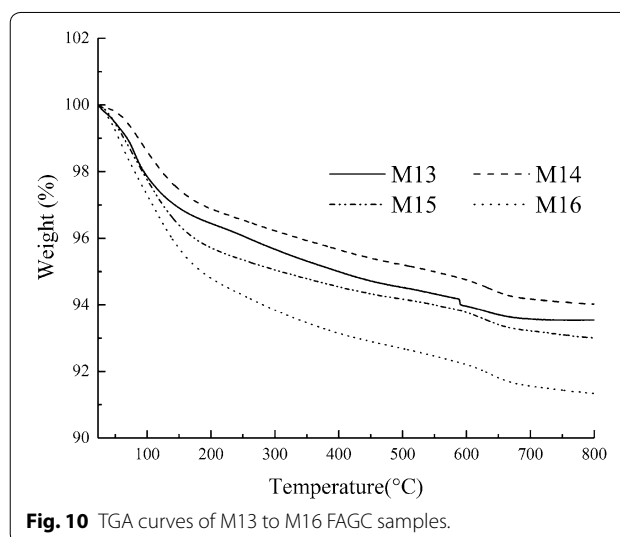
Table 7 Elements analysis of specimens in weight % and atom %.

Elements	M13 (spectrum 1)		M14 (spectrum 2)		M15 (spectrum 3)		M16 (spectrum 4)	
	Weight, %	Atom, %	Weight, %	Atom, %	Weight, %	Atom, %	Weight, %	Atom, %
O	47.24	57.96	51.15	60.55	45.7	58.73	42.43	56.92
Na	38.31	32.71	43.42	35.78	8.28	7.41	1.45	1.36
Al	1.39	1.01	0.73	0.51	11.06	8.43	20.45	16.27
Si	8.97	6.27	4.64	3.13	34.19	25.03	27.24	20.82
K	4.09	2.05	0.06	0.03	0.77	0.4	8.42	4.62
Total	100.00	100.00	100.00	100.00	100.00	100.00	100.00	100.00
Si/Al Ratio	6.45	6.21	6.36	6.14	3.09	2.97	1.33	1.28

Al atomic ratio are also given in Table 7. According to Davidovits, geopolymer is a kind of three-dimensional amorphous microstructural composition formulated by $M_2O \cdot mAl_2O_3 \cdot nSiO_2$, where M refers to alkali metals, $m \approx 1$ and $2 \leq n \leq 6$ (Davidovits 2008). Therefore, the range of Si/Al atomic ratio in geopolymer should be in the range of $1 \leq Si/Al \leq 3$. Together with the data in Table 7, the gel in Fig. 8c, d could be regarded as geopolymer. Much higher Na atomic content was detected in Fig. 8a, b, implying that the surface of geopolymer in Fig. 8a, b might be covered with some unreacted sodium compound (for example, unreacted sodium hydroxide and sodium silicate). Hence, more geopolymer was produced in M15 and M16 samples, causing higher long-term compressive strength. No trace of calcium element was detected in the samples, which shows that expansive sodium-calcium silicate gels were not formed in concrete. Therefore, this result indicates that low-calcium fly ash-based geopolymer concrete has lower possibility to suffer from deleterious alkali silica reaction (ASR).

3.4 Thermogravimetric Analysis

The results of thermogravimetric analysis (TGA) are illustrated in Fig. 10. It noticed from Fig. 10 that all the samples experienced an increase in the weight loss as the temperature increased. The rapid decline in the weight occurred before 200 °C was mainly due to the loss of free water and part of chemically combined water existing in FAGCs (Kong and Sanjayan 2010; Rashad 2015; Abdulkareem et al. 2014). After the quick weight loss, all the four mixtures experienced a gradual weight loss between 200 and 800 °C, which was related to the evaporation of chemically combined water that occurred up to 300 °C (Abdulkareem et al. 2014) and to the dehydroxylation of OH groups that occurred at temperatures above 300 °C (Duxson et al. 2007a, b). It can be seen from Fig. 10 that the weight losses of the four groups were different and the difference of weight loss began to be larger at about 150 °C. This indicates that different amounts

**Fig. 10** TGA curves of M13 to M16 FAGC samples.

of geopolymer gels were produced in these four groups, which was consistent with the results of SEM-EDS test. The weight loss of M13, M14, M15 and M16 after exposure to 800 °C was about 6.4%, 6.0%, 7.0% and 8.7%. The results showed that the weight loss reached the minimum (6.0%) with declining the SiO_2/Na_2O ratio to 1.7:1 from 2.0:1 and it then increased to 7.0% and 8.7% with declining the SiO_2/Na_2O ratios to 1.4:1 and 1.2:1, respectively.

The results of derivative thermogravimetry (DTG) are presented in Fig. 11. It can be observed from Fig. 11 that the first peak of M16 sample occurred at about 55.2 °C and the first peak of M13, M15 and M14 samples occurred at about 79.3 °C, 79.6 °C and 87.1 °C, respectively. The first peak represents the maximum weight loss rate, which was believed to be the evaporation of free water. All the four samples experienced faster weight loss rate up to 200 °C, after which a relatively gentle weight loss rate was observed. A second peak could be observed at about 632 °C in all the DTG curves, which is attributed to the dehydroxylation of sodium-based geopolymers ($Na_n\{-(SiO_2)_2AlO_2\}_n \cdot wH_2O$) (Duxson et al. 2007b).

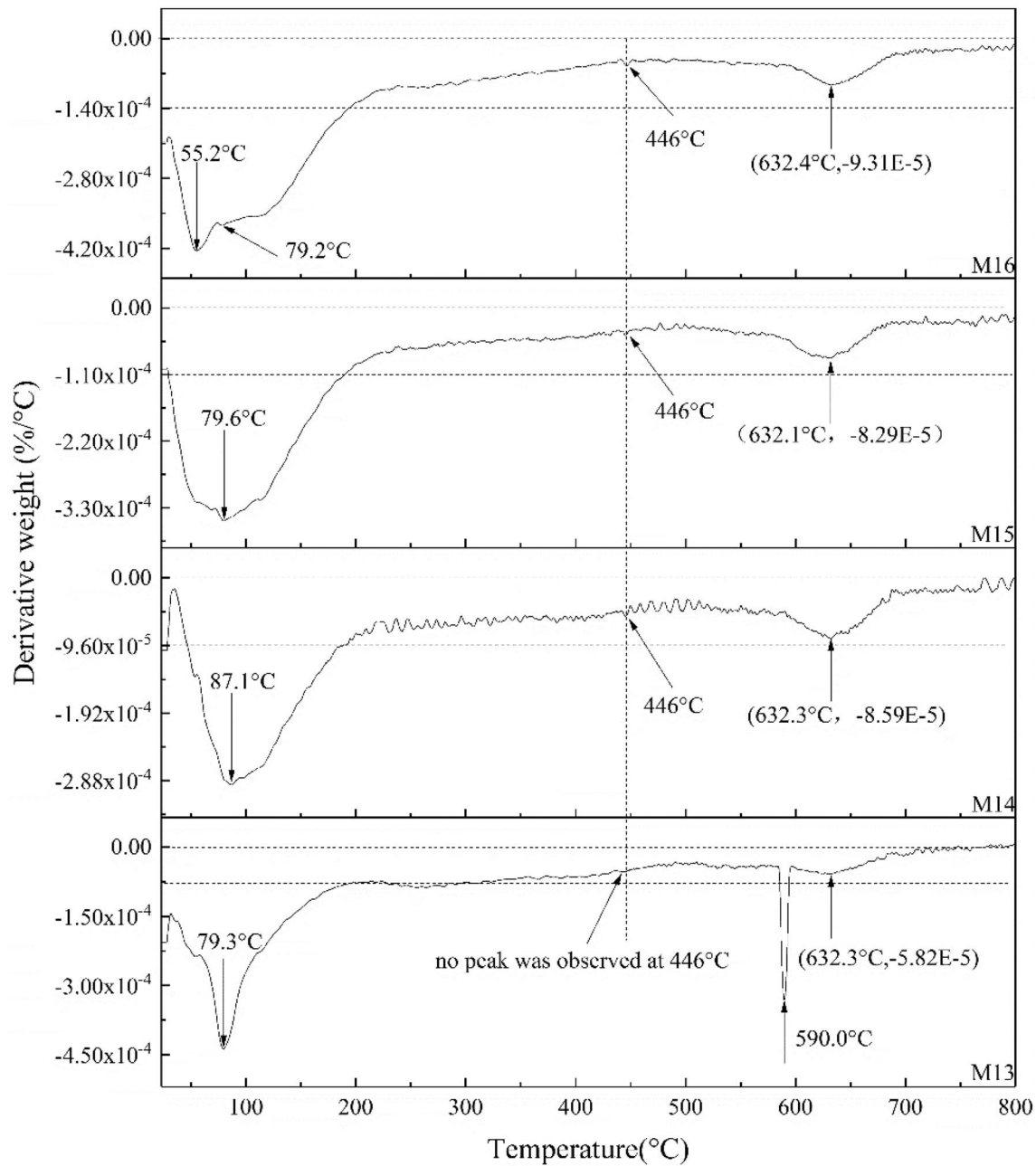


Fig. 11 DTG curves of M13 to M16 FAGC samples.

Due to the two distinct peaks, there were two step weight loss in all the TGA curves.

4 Property Development and Optimal Mixture Design of FAGC

4.1 Mechanism of Strength Development and Failure Analysis Under Compression

The compressive strength of FAGC increased with the increase of curing time because geopolymerization

continued to occur during the curing period. The continued geopolymerization could reduce the size and number of pores, diminish the width and number of cracks and enhance the strength of MAIZ, which was illustrated in Fig. 12.

The influence of HSC and L/FA ratio could be intuitively expressed by Eqs. (1) and (2) (Van Jaarsveld et al. 1997)

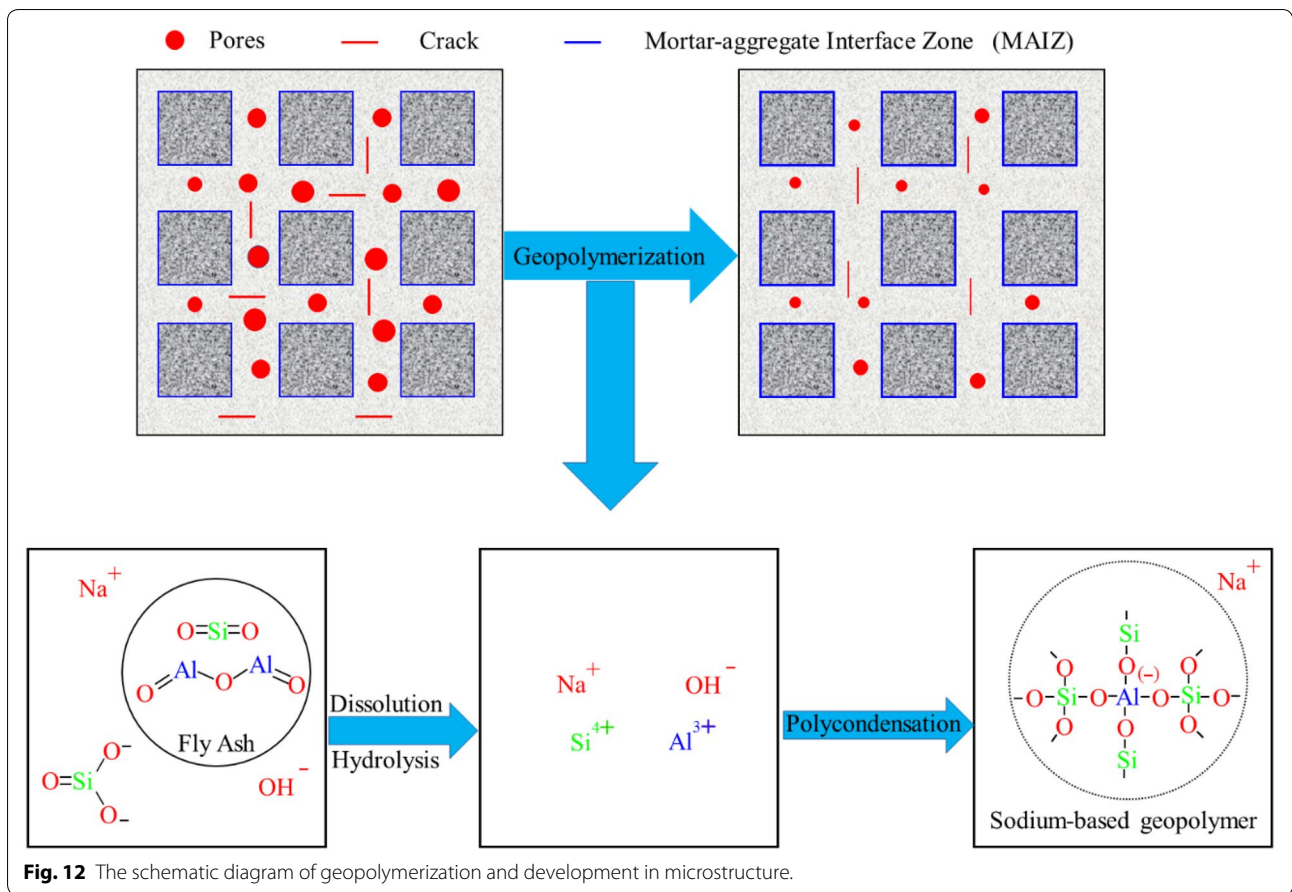
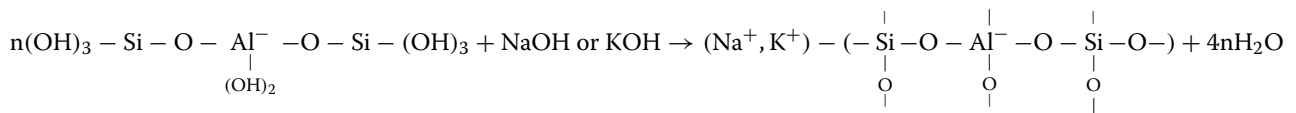
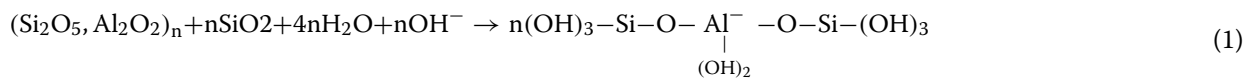


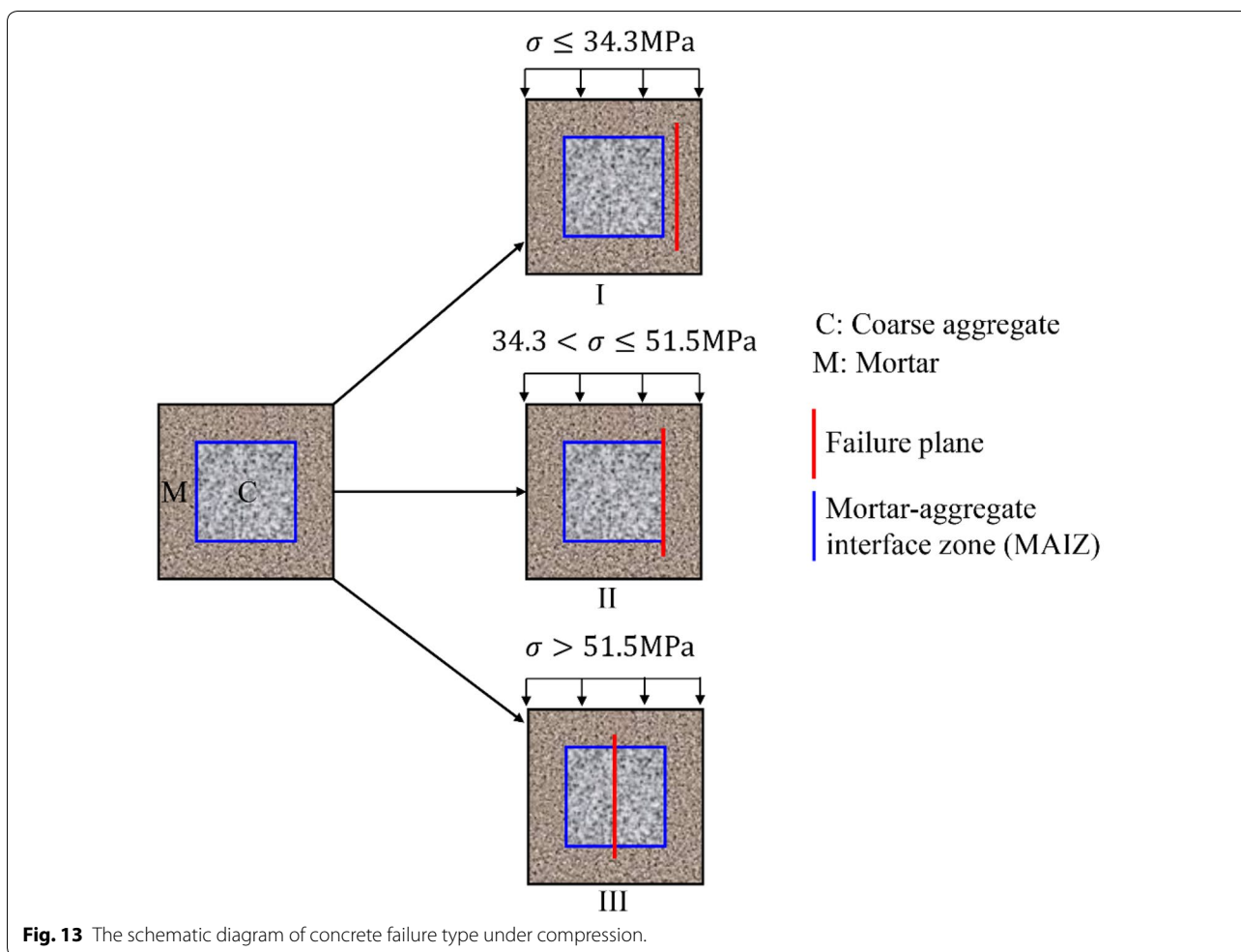
Fig. 12 The schematic diagram of geopolymerization and development in microstructure.



Geopolymeric structure
(2)

The NaOH solution of higher concentration had greater ability in the efficiency of activation (Zuhua et al. 2009) and higher SHC was more effective in dissolving the fly ash particles, leading to much more complete geopolymerization and improving the compressive strength. Hence the increase in SHC value made a greater contribution to a relatively high geopolymerization degree and resulted in higher compressive strength. Previous works (Weng and Sagoe-Crentsil 2007; Sagoe-Crentsil and Weng 2007) and Eq. (1) demonstrated that water was an important

medium for the destruction of raw materials and the transfer of effective ions. However, too much water would decrease the geopolymerization rate because of its dilution effect. Therefore, compressive strength increased with L/FA ratio below 0.44 and declined with the increase in the L/FA ratio in the range of from 0.44 to 0.52. Previous work (Sathonsaowaphak et al. 2009) proved that the compressive strength began to decline when the SS/SH ratio was larger than 2.0 because of the difficulty in compaction. Additionally, sodium silicate solution was a



combination of sodium silicate and distilled water. The increase in the ratio increased the water content existing in the alkaline solution, resulting in the decrease in the concentration of NaOH solution. As a result, the geopolymerization rate would be reduced and less N-A-S-H gels would be produced.

Figure 13 was used to conduct the failure analysis of FAGC under compression. Based on the results of Fig. 6, the concrete failure can be divided into three models (I, II and III) according to the position of failure plane. It was observed from Fig. 13 that the position of failure plane was related to the compressive strength of FAGCs. Generally, the failure plane occurred at the location of has the lowest strength. For example, the strength of mortar-aggregate interface zone (MAIZ) was the lowest in model II, therefore the concrete specimen was crushed because of the failure of MAIZ.

4.2 Optimal Mixture Design

4.2.1 Orthogonal Analysis Principle

The orthogonal analysis was used to gain the optimal geopolymer concrete mix. The analysis process consists of range analysis and variance analysis. The range analysis is used to determine the optimal level of each factor and assess the significance level of all factors. In the range analysis, the K value and R value are calculated. The K value of each level of a factor is the sum of four compressive strength values with the same level. Taking factor A for an example, the K_1 value is the sum of compressive strength of all specimens with L/FA of 0.40. The level of each factor with the largest K value has the most significant influence on compressive strength. The R value for each factor is the difference between the maximum and minimal K values of the four levels. The influence of one factor on the compressive strength

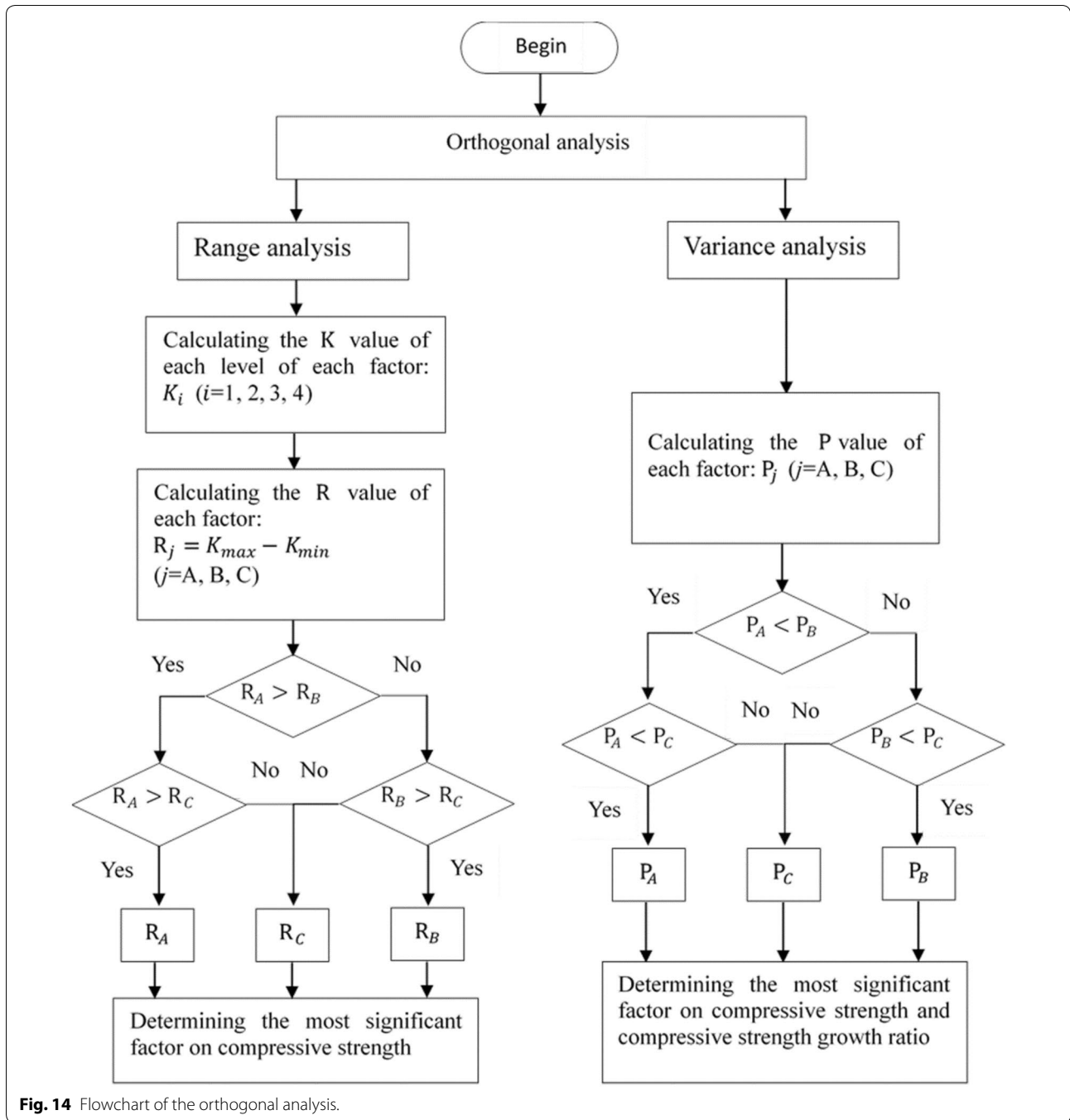


Fig. 14 Flowchart of the orthogonal analysis.

would be the most significant if it has the largest R value. The variance analysis is conducted to calculate the P -value of each factor. The most significant factor has the smallest P -value. The orthogonal analysis process is also illustrated using the following flowchart (Fig. 14).

4.2.2 Results of Orthogonal Analysis and Optimal Mixture Design

The 7-day compressive strength and 28-day compressive strength (Table 6) were selected to conduct the range analysis. The results of range analysis are summarized in Table 8.

Table 8 The range analysis on initial and long-term compressive strength.

Factors	7-day compressive strength			28-day compressive strength			480-day compressive strength		
	A (L/FA)	B (SHC)	C (SS/SH)	A (L/FA)	B (SHC)	C (SS/SH)	A (L/FA)	B (SHC)	C (SS/SH)
K_1	199.3	134.7	227.1	211.5	142.8	238.4	260.5	178.7	284.6
K_2	218.0	184.7	218.3	224.8	197.1	230.0	265.3	240.6	280.4
K_3	207.6	228.7	192.9	221.7	243.3	210.1	272.4	297.1	255.6
K_4	183.8	260.6	159.9	193.8	268.6	173.6	245.8	327.6	223.4
K	808.7	808.7	808.7	851.8	851.8	851.8	1044.0	1044.0	1044.0
R	34.2	125.8	71.7	31.1	125.8	64.8	26.6	149.0	61.2

In Table 8, K_1 value equals to the sum of compressive strength of all specimens with level 1 of each factor. K value and R value are calculated as Eq. (3) and Eq. (4).

$$K = K_1 + K_2 + K_3 + K_4 \tag{3}$$

$$R = \text{Max} [K_1, K_2, K_3, K_4] - \text{Min} [K_1, K_2, K_3, K_4] \tag{4}$$

It is observed from Table 8 that the influence of SHC factor on initial and long-term compressive strength is the most significant because of its largest R value. As the SHC value increased from 8 M to 14 M, the 7-day, 28-day and 480-day compressive strength increased 95.4%, 86.9% and 83.37% respectively. It was also observed from Table 8 that the K value of factor B increased with the molarity of NaOH solution, indicating that the compressive strength of FAGC tended to increase with the increase of NaOH molarity. As the SS/SH ratio increased from 2.0 to 4.0, the 7-day, 28-day and 480-day compressive strength reduced 29.6%, 27.2% and 21.5%, respectively. The K value of factor C declined with the ratio of SS/SH, which could be obtained from Table 8. It demonstrated that an increase in the ratio of SS/SH resulted in the decline of initial and long-term compressive strength. Table 8 shows that the K value of factor A reached its maximum when the L/FA ratio was 0.44. The K value of factor A increased with the increase of L/FA ratio when the ratio was smaller than 0.44 and then decreased with the increase of the ratio when the ratio was larger than 0.44. This result indicates that initial and long-term

compressive strength of FAGC reached its maximum when the L/FA ratio was 0.44.

The variance analysis which is involved in large numbers of mathematics calculation was conducted using the SPSS software. The sum of squares (SS), degree of freedom (DF), F value (F) and P -value (P) are presented in Table 9. The influence of the factor on compressive strength would be more significant if the P -value of each factor was smaller. As shown in Table 9, the P -value of factor B was the smallest followed by those of factors C and A. Therefore, the influence of sodium hydroxide concentration (SHC) on compressive strength was much more significant than the other two factors. Additionally, the P -values of the three factors at all the testing ages are also presented in Fig. 15. The P -values of factor A were the biggest during all the curing ages. Therefore, the influence of L/FA ratio ranging from 0.4 to 0.52 on compressive strength of geopolymer concrete was not as significant as the influence of water to cement ratio on compressive strength of traditional cement-based concrete. However, L/FA ratio played a vital role in providing an essential liquid environment for geopolymerization.

The results of 28-day, 60-day, 100-day and 480-day compressive strength subtracted 7-day compressive strength were calculated as compressive strength growth ratio. The P -values of various factors on the compressive strength growth ratio are shown in Fig. 16. The P -value of factor B was the largest during all the curing days and it reached 0.878 at 480 days. The results indicate that the influence of concentration of NaOH solution made very

Table 9 The variance analysis on 7- and 28-day compressive strength.

Sources of variation	7-day compressive strength				28-day compressive strength			
	SS	DF	F	P	SS	DF	F	P
A(L/FA)	193.1	3	0.257	0.855	160.8	3	0.218	0.882
B(SHC)	2133.2	3	7.964	0.003	2239.3	3	10.135	0.001
C (SS/SH)	731.3	3	1.183	0.357	616.6	3	0.986	0.432
Error	3.654	3	1.0	0.5	3.604	3	1.0	0.5



Fig. 15 P-value of different factors on compressive strength.

little difference to the strength enhancement with age after the initial heat curing, which was distinctly different from its significant influence on the initial strength. The figure also shows that the *P*-value of factor C decreased with the curing days, indicating that the influence of SS/SH ratio on compressive strength growth ratio became more and more significant with the increase of age.

On the basis of range analysis, the optimal mixture was A2B4C1, which meant that L/FA ratio was at level 2, SHC was at level 4 and SS/SH ratio was at level 1.

5 Conclusion

This study quantitatively assessed the influence of three important factors on the compressive strength and rate of compressive strength increase over the long term up to 480 curing days. The following conclusions are drawn from this study:

1. The initial compressive strength was higher for using higher concentration of NaOH solution. However, the rate of compressive strength increase over the

long term was low for the mixtures using higher concentration of NaOH solution.

2. The initial and long-term compressive strength decreased with the increase of SS/SH ratio. Even though the SS/SH ratio showed a small effect on the initial compressive strength, it showed a significant effect on the rate of compressive strength increase over the long term.
3. The initial and long-term compressive strength showed an increasing trend with the increase of liquid to fly ash ratio of up to 0.44 and then showed a decreasing trend with the increase of liquid to fly ash ratio.
4. The 480-day compressive strength of FAGC increased with the increase of the $\text{Na}_2\text{O}/\text{SiO}_2$ molar ratio. Also, the 480-day compressive strength increased with the increase in Si/Al molar ratio of up to 1.87 and was observed to decline when the Si/Al molar ratio was greater than 1.87.
5. Based on the failure modes of concrete, the long-term compressive strength of FAGC was found to be associated with the strength of the mortar–aggregate interfacial zone (MAIZ).

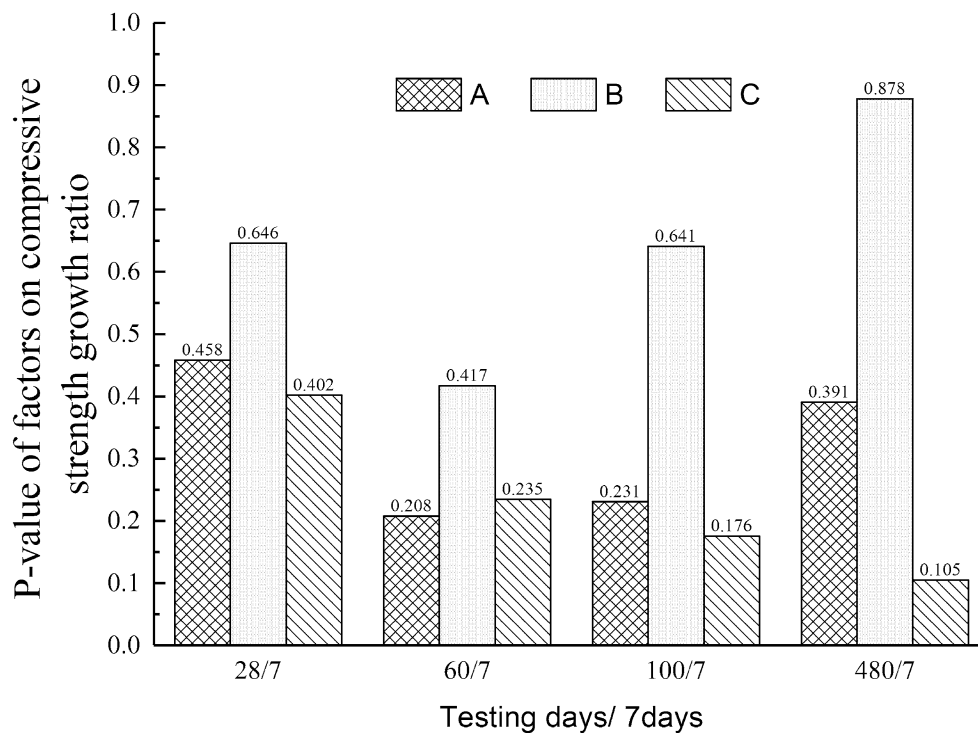


Fig. 16 P-value of various factors on strength growth ratio with regard to 7-day strength.

6. Based on theoretical analysis of the results of OED method, the optimum mixture was found as A2B4C1, which represents L/FA ratio at level 2, SHC at level 4 and SS/SH ratio at level 1.

Acknowledgments

The authors also like to thank He Yi of the Analytical & Testing Center (ATC) of Sichuan University for his great help in the SEM–EDS tests. The first author is supported by the China Scholarship Council (CSC), which is sincerely appreciated.

Authors' contributions

All authors contributed equally to this paper. All authors read and approved the final manuscript.

Funding

This research was funded by the Program for Changjiang Scholars and Innovative Research Team (IRT14R37), the National Natural Science Foundation of China (51208325) and the Science & Technology Support Program of Sichuan Province (No.2015GZ0245 and No.2015JPT0001).

Availability of data and materials

The authors agree to share their data.

Competing interests

The authors declare that they have no competing interests.

Author details

¹ Key Laboratory of Deep Underground Science and Engineering (Ministry of Education), School of Architecture and Environment, Sichuan University, Chengdu 610065, China. ² Department of Civil Engineering, Curtin University, GPO Box U1987, Perth, WA 6845, Australia. ³ School of Mechanical

Engineering, Chengdu University, Chengdu 610106, China. ⁴ Laboratoire de Tribologie et de Dynamique des Systèmes (LTDS), Ecole Nationale d'Ingénieurs de Saint-Etienne (ENISE), Univ Lyon, UMR 5513, 58 Rue Jean Parot, 42023 Saint-Etienne Cedex 2, France.

Received: 31 May 2019 Accepted: 24 September 2019

Published online: 30 December 2019

References

- Abdulkareem, O. A., Al Bakri, A. M., Kamarudin, H., Nizar, I. K., & Alal'eddin, A. S. (2014). Effects of elevated temperatures on the thermal behavior and mechanical performance of fly ash geopolymer paste, mortar and light-weight concrete. *Construction and Building Materials*, *50*, 377–387.
- Chi, M., & Huang, R. (2013). Binding mechanism and properties of alkali-activated fly ash/slag mortars. *Construction and Building Materials*, *40*, 291–298.
- Chithambaram, S. J., Kumar, S., Prasad, M. M., & Adak, D. (2018). Effect of parameters on the compressive strength of fly ash based geopolymer concrete. *Structural Concrete*, *19*, 1202–1209.
- Davidovits, J. (2008). *Geopolymer chemistry and applications*. Saint-Quentin: Geopolymer Institute.
- De Vargas, A. S., Dal Molin, D. C., Vilela, A. C., Da Silva, F. J., Pavao, B., & Veit, H. (2011). The effects of Na₂O/SiO₂ molar ratio, curing temperature and age on compressive strength, morphology and microstructure of alkali-activated fly ash-based geopolymers. *Cement & Concrete Composites*, *33*, 653–660.
- Duxson, P., Lukey, G. C., & van Deventer, J. S. J. (2007a). Physical evolution of Na-geopolymer derived from metakaolin up to 1000 C. *Journal of Materials Science*, *42*, 3044–3054.
- Duxson, P., Lukey, G. C., & van Deventer, J. S. J. (2007b). The thermal evolution of metakaolin geopolymers: Part 2—Phase stability and structural development. *Journal of Non-Crystalline Solids*, *353*, 2186–2200.

- Gunasekara, C., Sujeeva, S., & Law, D. W. (2017). Long-term mechanical properties of different fly ash geopolymers. *ACI Structural Journal*. <https://doi.org/10.14359/51689454>.
- Heah, C. Y., Kamarudin, H., Al Bakri, A. M., Bnhussain, M., Luqman, M., Nizar, I. K., et al. (2012). Study on solids-to-liquid and alkaline activator ratios on kaolin-based geopolymers. *Construction and Building Materials*, *35*, 912–922.
- Hongen, Z., Feng, J., Qingyuan, W., Ling, T., & Xiaoshuang, S. (2017). Influence of cement on properties of fly-ash-based concrete. *ACI Materials Journal*, *114*, 745–753.
- Ji, L., Si, Y., Liu, H., Song, X., Zhu, W., & Zhu, A. (2014). Application of orthogonal experimental design in synthesis of mesoporous bioactive glass. *Microporous and Mesoporous Materials*, *184*, 122–126.
- Jo, B. W., Chakraborty, S., Choi, J. S., & Jo, J. H. (2016). Investigation on the effectiveness of aqueous carbonated lime in producing an alternative cementitious material. *International Journal of Concrete Structures and Materials*, *10*, 15–28.
- Kong, D. L. Y., & Sanjayan, J. G. (2010). Effect of elevated temperatures on geopolymer paste, mortar and concrete. *Cement and Concrete Research*, *40*, 334–339.
- Kotwal, A. R., Kim, Y. J., Hu, J., & Sriraman, V. (2015). Characterization and early age physical properties of ambient cured geopolymer mortar based on class C fly ash. *International Journal of Concrete Structures and Materials*, *9*, 35–43.
- Ministry of Construction of the PRC & General Administration of Quality Supervision, Inspection and Quarantine of the People's Republic of China (2003). GB/T 50081-2002 standard for test method of mechanical properties on ordinary concrete (Chinese standard), Beijing.
- Nath, P., & Sarker, P. K. (2015). Use of OPC to improve setting and early strength properties of low calcium fly ash geopolymer concrete cured at room temperature. *Cement & Concrete Composites*, *55*, 205–214.
- Nazari, A., Bagheri, A., Sanjayan, J. G., Dao, M., Mallawa, C., Zannis, P., et al. (2019). Thermal shock reactions of Ordinary Portland cement and geopolymer concrete: Microstructural and mechanical investigation. *Construction and Building Materials*, *196*, 492–498.
- Pasupathy, K., Berndt, M., Sanjayan, J., Rajeev, P., & Cheema, D. S. (2018). Durability performance of precast fly ash-based geopolymer concrete under atmospheric exposure conditions. *Journal of Materials in Civil Engineering*, *30*, 04018007.
- Rashad, A. M. (2015). Potential use of phosphogypsum in alkali-activated fly ash under the effects of elevated temperatures and thermal shock cycles. *Journal of Cleaner Production*, *87*, 717–725.
- Riahi, S., & Nazari, A. (2012). The effects of nanoparticles on early age compressive strength of ash-based geopolymers. *Ceramics International*, *38*, 4467–4476.
- Sagoe-Crentsil, K., & Weng, L. (2007). Dissolution processes, hydrolysis and condensation reactions during geopolymer synthesis: Part II. High Si/Al ratio systems. *Journal of Materials Science*, *42*, 3007–3014.
- Sathonsaowaphak, A., Chindapasirt, P., & Pimraksa, K. (2009). Workability and strength of lignite bottom ash geopolymer mortar. *Journal of Hazardous Materials*, *168*, 44–50.
- Shi, X. S., Collins, F. G., Zhao, X. L., & Wang, Q. Y. (2012). Mechanical properties and microstructure analysis of fly ash geopolymer recycled concrete. *Journal of Hazardous Materials*, *237–238*, 20–29.
- Sindhunata, J. S. J., Van Deventer, J. S., Lukey, G. C., & Xu, H. (2006). Effect of curing temperature and silicate concentration on fly-ash-based geopolymerization. *Industrial and Engineering Chemistry Research*, *45*, 3559–3568.
- Van Jaarsveld, J. G. S., Van Deventer, J. S. J., & Lorenzen, L. (1997). The potential use of geopolymeric materials to immobilise toxic metals: Part I. *Theory and applications; Minerals engineering*, *10*, 659–669.
- Weng, L., & Sagoe-Crentsil, K. (2007). Dissolution processes, hydrolysis and condensation reactions during geopolymer synthesis: Part I—Low Si/Al ratio systems. *Journal of Materials Science*, *42*, 2997–3006.
- Xu, H., Van Deventer, J. S. J., & Lukey, G. C. (2001). Effect of alkali metals on the preferential geopolymerization of stilbite/kaolinite mixtures. *Industrial and Engineering Chemistry Research*, *40*, 3749–3756.
- Yang, P., Tan, X., Sun, H., Chen, D., & Li, C. (2011). Fire accident reconstruction based on LES field model by using orthogonal experimental design method. *Advances in Engineering Software*, *42*, 954–962.
- Zhang, H., Shi, X., & Wang, Q. (2018). Effect of curing condition on compressive strength of fly ash geopolymer concrete. *ACI Materials Journal*, *115*, 191–196.
- Zhu, J., Chew, D. A. S., Lv, S., & Wu, W. (2013). Optimization method for building envelope design to minimize carbon emissions of building operational energy consumption using orthogonal experimental design (OED). *Habitat International*, *37*, 148–154.
- Zuhua, Z., Xiao, Y., Huajun, Z., & Yue, C. (2009). Role of water in the synthesis of calcined kaolin-based geopolymer. *Applied Clay Science*, *43*, 218–223.

Publisher's Note

Springer Nature remains neutral with regard to jurisdictional claims in published maps and institutional affiliations.

Submit your manuscript to a SpringerOpen® journal and benefit from:

- Convenient online submission
- Rigorous peer review
- Open access: articles freely available online
- High visibility within the field
- Retaining the copyright to your article

Submit your next manuscript at ► [springeropen.com](https://www.springeropen.com)